FERMILAB-PUB-79-135-E #3444

Experimental Determination of Elastic and Topological Cross Sections in 48.9 GeV/c $\bar{p}p$ Interactions*

D. E. Zissa, V. E. Barnes, D. D. Carmony, L. J. Dauwe, J. A. Gaidos, L. J. Gutay, A. T. Laasanen, R. L. McIlwain, D. H. Miller, L. K. Rangan, R. M. Robertson, and R. B. Willmann

Department of Physics, Purdue University, West Lafayette, Indiana 47907, U.S.A.

and

F. Turkot

Fermi National Accelerator Laboratory, Batavia, Illinois 60510, U.S.A.

Abstract

The elastic and topological $\bar{p}p$ cross sections have been measured at 48.9 GeV/c in the Fermilab Proportional Wire Chamber 30-Inch Bubble Chamber Hybrid Spectrometer. The elastic cross section is 7.81 ± 0.24 mb and the slope of the elastic differential cross section at $t = 0$ is 13.4 ± 0.8 GeV^{-2}. Further, the moments of the inelastic topological cross section distribution are $\langle n_c \rangle = 5.69 \pm 0.03$, $\langle n_c \rangle / D = 2.10 \pm 0.02$, and $f_2^{cc} = 1.67 \pm 0.12$.

*Supported in part by the United States Department of Energy.

The nature of high energy antiproton-proton interactions and their relation to proton-proton interactions are not yet fully understood [1]. Until recently, experimental study of $\bar{p}p$ interactions at high energies has been hindered by the unavailability of $\bar{p}$ beams. Moreover, the annihilation process becomes increasingly difficult to study as its cross section falls rapidly with increasing energy. The former difficulty has been overcome with an enriched $\bar{p}$ beam, and the study of high energy $\bar{p}p$ annihilation has been optimized by choosing 50 GeV/c beam energy, where the annihilation process is expected to be greater than 10% of the total $\bar{p}p$ cross section, and where hadronic interactions are entering the high energy regime. In this paper we present a study of some features of the $\bar{p}p$ charged multiplicity distribution at 50 GeV/c and make comparisons with $\bar{p}p$ and pp interactions at energies between 3 GeV and 400 GeV. In the accompanying paper we discuss the $\bar{p}p$ - pp topological cross section differences.

The results are derived from a sample of 92 000 pictures taken in the Fermilab Proportional Wire Chamber 30-Inch Bubble Chamber Hybrid Spectrometer (PWHS) [2]. The beam incident upon the hydrogen filled rapid cycling bubble chamber was created by a novel antiproton enrichment scheme, first proposed by W. Neale [3], which was modified for greater $\bar{p}$ yield [4]. The 400 GeV/c extracted proton beam from the accelerator was focused onto a copper target located halfway along the bore of a ten foot long sweeping magnet, which removed all charged particles emerging from the target. Antilambdas and other neutral particles that decayed, after emerging from the magnet at 6 milliradians, were the source of the beam which contained 30% antiprotons. The remainder of the beam consisted primarily of negative pions from the decay of K^o's and Λ^o's. A bubble chamber

photograph was taken only if two or more antiproton beam particles entered the chamber, resulting in an effective flux of $\sim$ 42% antiprotons. As a result of this antiproton enrichment scheme, 57% of the observed interactions were induced by antiprotons.

The antiprotons were tagged by a Cerenkov counter operated in a threshold mode, and the antiproton events contain a 3% background from mistagged pion induced events[†1]. Three triplets of upstream Proportional Wire Chambers (PWC) accurately determined the beam position and direction in the bubble chamber. The beam momentum was determined to be 48.9 $\pm$ 0.5 GeV/c by swimming 1700 beam tracks from the upstream PWC's through the bubble chamber magnetic field to the downstream wire chambers, as in [5]. The quoted error in the beam momentum is dominated by uncertainties in the magnetic fringe field.

Events of all topologies, including those with V^o's and γ's pointing to the event vertex, were scanned and measured using Scanning and Measuring Projectors with online Three View Geometry Program (TVGP). An effective track reconstruction efficiency of approximately 99% was obtained with this system. A second independent scan was done on 20% of the film distributed evenly throughout the experiment. Separate single scanning efficiencies were found for the following categories: zero prongs without associated neutrals (75 $\pm$ 25%), two prongs without associated neutrons (85 $\pm$ 2%), and all other events (91 $\pm$ 1%).

[†1] A comparison of the beam tagging Cerenkov counter and another Cerenkov counter for the last quarter of the run showed that the antiproton signal included a 6% background (mostly consisting of negative pions). Taking into account π^- decay between the tagging Cerenkov and the bubble chamber and the $\pi^-/\bar{p}$ cross section ratio, a 3% background in the antiproton event sample was calculated.

The ionization bubble density of each measured positive track with momentum less than 1.33 GeV/c was examined to obtain identification of slow protons and pions. The tracks unidentifiable by ionization were treated as pions unless they were otherwise identified by a four constraint kinematic fit. No conflict was found between kinematic fits to elastic scattering (see below) and the bubble density identification.

The four downstream PWC's located two to six meters from the center of the bubble chamber utilized the bubble chamber fringe field and the increased lever arm to improve the momentum measurement of fast secondary tracks. The Proportional Wire Geometry Program (PWGP) [6] was used to construct upstream and downstream wire chamber tracks. The program HOOKUP [7] was used to combine the bubble chamber and wire chamber data. An event was called a tagged $\bar{p}$ event only if the bubble chamber beam track matched in intercept and angle with an upstream wire chamber track associated with a null Cerenkov signal. Wherever possible links were established between secondary tracks in the bubble chamber and the downstream PWC's when the bubble chamber measured momenta were greater than 15 GeV/c. About 45% of the tracks with measured momenta between 15 and 25 GeV/c and about 70% of the tracks with measured momenta above 25 GeV/c were successfully linked with secondaries. The momentum resolution was 7-10% for the linked secondaries. The bare bubble chamber information was used if there was no hookup.

Determination of the elastic cross section and the total number of events: The elastic reaction hypothesis was tried for all 2569 measured two prong events using the SQUAW kinematic fitting program. Instead of the usual four momentum conservation, SQUAW was modified to conserve $\vec{p}$ and $E - \vec{p}\cdot\hat{n}$ where $\hat{n}$ is a unit vector in the incident beam direction. Events

having a four constraint (4C) chi-square of less than 30 were selected as elastic events. A few of the true elastic event failed to satisfy the above criterion after the first pass of measurements. In order to find additional candidates for elastic events, a remeasurement list was made (a) from the high χ^2 tail of the 4C elastic distribution, (b) from 3C elastic fits where the momentum of the fast track was deleted, (c) from 4C fits obtained by dropping one of the three stereoscopic views, (d) and from events having a downstream wire hit compatible with the calculated direction of the fast elastic recoil track. Events which passed the 4C criterion after remeasurement were added to the elastic sample. This procedure resulted in a 10% addition to the initial elastic sample. Criterion (d) alone yields an 8% addition to the initial elastic sample.

To determine the elastic cross section and the total number of events, the following corrections were made:

(1) The inelastic event background in the sample selected as elastic events was measured as follows: (a) The contamination from multineutral events was found to be negligible by attempting to fit four prong events with two tracks omitted. (b) It was found that two of the two prong events with associated gammas passed the elastic selection criterion. Assuming that one π^o was produced in each event and using the probability of pair conversion in the bubble chamber, a total contamination of $2.4 \pm 1.7\%$ was calculated.

(2) Both elastic and inelastic two prong events with small four momentum transfer squared (t) tended to be missed in both scans if the recoil proton track pointed toward or away from the cameras. Therefore, the distributions of the proton azimuthal angle about the beam direction

were repopulated separately for the five t-intervals in the range $0.04 \leq -t \leq 0.14$ GeV^2.

(3) In order to determine the number of elastic events with $-t \leq 0.04$ GeV^2, the elastic differential distribution was fitted to the form $A \exp(Bt + Ct^2)$ in the interval $0.04 \leq -t \leq 0.30$ GeV^2.

(4) After the initial fit and the low t correction were made, the resulting total number of events was used along with $\sigma_T = 43.86 \pm 0.25$ mb [8][†2] and the optical theorem to compute the number of events (dN_{el}/dt) at $t = 0$. Imposing the condition that the fit passes through this point within its error of 1.5% relative to our data, the above procedure was iterated until consistency was obtained.

Using these procedures the elastic and topological cross sections were obtained, normalized to the above total cross section from Ref. [8].[†2] In particular it was found that $\sigma_{el} = 7.81 \pm 0.24$ mb, where the uncertainties in all of the corrections have been folded in. The fitted parameters are:

$$A = 98.5 \pm 1.5 \text{ mb GeV}^{-2}$$

$$B = 13.4 \pm 0.8 \text{ GeV}^{-2}$$

$$C = 4.4 \pm 3.9 \text{ GeV}^{-4}$$

Figure 1 shows the elastic data along with the fit. The value of A reflects the optical point and therefore the counter data. The values of B and C reflect the data of this experiment and agree well with the parameters measured by Ayres, et al. [9].

[†2]The total cross section σ_T was determined to be 44.9 ± 1.2 mb, using 20% of the film. This result is in good agreement with that of A. S. Carroll, et al., [8], $\sigma_T = 43.86 \pm 0.25$ mb at 50 GeV/c.

Determination of the multiplicity cross sections: First, corrections were made to each charged multiplicity cross section for undetected Dalitz pairs. Neutral strange particle decays and γ conversions were measured and constrained kinematic fits were attempted assuming that the neutral particles originated from the primary event vertex. Gammas were weighted by the probability of converting in a cylindrical fiducial volume of radius 30 cm, and it was assumed that all gammas arose from π^o decay, and that the scanning efficiency for pairs was 100%. Using the π^o Dalitz decay branching ratio of 1.15%, it is estimated that about 200 out of 10 000 events have Dalitz pairs (for $\sim$ 1/3 of these events the Dalitz pair was found in scanning). The charged multiplicity cross sections were adjusted according to the number of Dalitz pairs estimated in each topology. Odd prong events were moved to the next higher multiplicity on the assumption that a short track was not visible. Vees and γ conversions near the vertex can be confused with charged tracks at the vertex; however, it was determined that this effect is negligible. Furthermore, no corrections were found necessary for unseen secondary interactions which produce extra charged tracks near the event vertex.

All of the above corrections having been incorporated, the topological cross sections listed in Table I were obtained. The errors reflect the statistical uncertainties in the numbers of events found as well as the uncertainties in the above corrections and in the low t elastic events. Also shown in Table I are moments of the inelastic charged multiplicity distribution. Errors were computed using all correlation terms in the error matrix. In Fig. 2 the 48.9 GeV/c topological cross sections are plotted together with published data at different beam momenta [10]. The solid curves are to guide the eye. The zero-prong cross section above 14 GeV/c is seen to

decrease steeply as $\sim p_{LAB}^{-(1.45 \pm .14)}$. The 2- and 4- prong cross sections decrease monotonically with p_{LAB} over the whole range of the figure from 2.5 GeV/c up to 100 GeV/c. Eight and higher prong cross sections rise monotonically, and are seen to continue to rise between 50 and 100 GeV/c. In particular, the 18- and 20-prong cross sections are rising very steeply at the highest measured energies. The six-prong cross section is seen to peak in the vicinity of 30 GeV/c, and the average charged multiplicity $\langle n_c \rangle$ passes through a value of 6.0 near 60 GeV/c. It will be interesting to see whether the eight-prong cross section behaves similarly by peaking somewhat before the value of p_{LAB} for which $\langle n_c \rangle = 8.0$. The data for proton-proton collisions [11] are certainly compatible with such a pattern.

The average charged multiplicity $\langle n_c \rangle$, the dispersion D, and the ratio $\langle n_c \rangle / D$ are shown in Figs. 3 a, b, and c, and are compared with data at a series of other momenta [12]. Our data fall on smooth curves through the previous data including the 32 GeV/c and 100 GeV/c points. In the highest measured momentum range, 50 GeV/c and above, the values of $\langle n_c \rangle$ for $\bar{p}p$ and for pp collisions may be slowly approaching each other, but higher energy $\bar{p}p$ data are required to determine if they converge. The values of D apparently converge before 200 GeV/c, which may be caused in part by the decrease with energy of the annihilation component of the $\bar{p}p$ multiplicity distribution. The ratios $\langle n_c \rangle / D$ appear to have converged already by 50 GeV/c, and there are indications that the value for $\bar{p}p$ interactions may begin to exceed the value for pp interactions. In the region, $3 \leq p_{LAB} \leq 50$ GeV/c, this ratio for $\bar{p}p$ interactions is approximately constant (~ 2) although it is increasing slowly, whereas $\langle n_c \rangle / D$ for pp interactions is decreasing rapidly with increasing beam momentum.

We have compared our data to the KNO scaling curve (not shown) fitted to pp data between 50 and 303 GeV/c [13]. Our $\bar{p}p$ distribution is slightly narrower than the KNO curve fit for the high energy pp data since the width $D/\langle n_c \rangle$ is smaller for our data.

A study of the difference between $\bar{p}p$ and pp topological cross sections will be presented in the following paper.

We would like to thank S. Pruss, M. Johnson, and W. Neale for helping to carry out the 40-60 GeV/c $\bar{p}$ beam feasibility test. Further, we would like to thank L. Stutte and R. Stefansky for their help with the beam and D. Theriot for his interest and support. The cooperation of the neutrino lab technical staff in the design and fabrication of the target and associated vacuum system is appreciated. We express our gratitude to the Hybrid Spectrometer Consortium and in particular to R. K. Yamamoto, J. Brau, and A. Napier, for maintaining their downstream chambers and the online computer during our experiment. Finally, we thank members of the Purdue scanning and measuring staff for their part in the analysis of the film.

REFERENCES

[1] Y. Eylon and H. Harari, Nucl. Phys. B80 (1974) 349.

[2] D. Fong, et al. Phys. Letters 53B (1974) 290, and references therein; D. Fong, et al. Nucl. Phys. B102 (1976) 386, and references therein.

[3] W. W. Neale, Enriched Particle Beams for the Bubble Chambers at FNAL, FNAL FN-259 (1974).

[4] V. E. Barnes et al., Tests of Antiproton Yield and Purity at 40, 50 and 60 GeV in the FNAL N3 Beam, Memo Nos. 350 and 351, High Energy Physics Notes, Purdue University (1975).

[5] W. M. Bugg, Brief Summary of Survey Results for Experiment 154, Newsnote, University of Tennessee (August 1974); W. M. Bugg, Utility Programs and System Performance; Experiment 154 Runs, Newsnote 28, University of Tennessee (1974).

[6] D. Fong, T. W. Ludlam, T. L. Watts, Secondary Track Measurement Using Multiwire Proportional Counters with the NAL 30-Inch Bubble Chamber, PHS Consortium Newsnote No. 36 (1973).

[7] J. T. Carroll, BC Note No. 16, SLAC (1972); W. M. Morse, Thesis, Purdue University (1975).

[8] A. S. Carroll et al., Phys. Rev. Letters 33 (1974) 928.

[9] D. S. Ayres et al., Phys. Rev. D15 (1977) 3105.

[10] 2.45 and 2.9 GeV/c: R. J. Abrams et al., Phys. Rev. D1 (1970) 1917; D. L. Parker et al., Nucl. Phys. B32 (1971) 29; P. S. Eastman et al., Nucl. Phys. B51 (1973) 29;

3.28 and 3.66 GeV/c: T. Ferbel et al., Phys. Rev. 137 (1965) B1250;

4.6 GeV/c: E. Bracci et al., CERN/HERA 73-1; D. Everett et al., Nucl. Phys. B73 (1974) 449;

5.7 GeV/c: K. Böckmann et al., Nuovo Cimento 42A (1966) 954;

6.94 GeV/c: T. Kitagaki et al., Phys. Rev. Letters 21 (1968) 175; T. Ferbel et al., Phys. Rev. 173 (1968) 1307.

12 GeV/c: W. Galbraith et al., Phys. Rev. 138 (1965) B913; K. J. Foley et al., Phys. Rev. Letters 11 (1963) 503; I. Borecka et al., Nuovo Cimento 5A (1971) 19;

14.75 GeV/c: W. Galbraith et al., op. cit.; K. J. Foley et al., op. cit.; D. Birnbaum et al., Phys. Rev. Letters 23 (1969) 663; F. T. Dao et al., Phys. Letters 51B (1974) 505;

22.4 GeV/c: E. Bracci et al., op. cit.: Yu. M. Antipov et al., Nucl. Phys. B57 (1973) 333; L. N. Abesalashvili et al., Phys. Letters 52B (1974) 236;

32 GeV/c: S. P. Denisov et al., Phys. Letters 36B (1971) 528; M. A. Jabiol et al., Nucl. Phys. B127 (1977) 365;

100 GeV/c: A. S. Carroll et al., Phys. Rev. Letters 33 (1974) 928, 932; R. E. Ansorge et al., Phys. Letters 59B (1975) 299.

[11] J. Frøyland and O. Skontorp, Nucl. Phys. B68 (1974) 93.

[12] Compilation of inelastic charged multiplicity data on $\pi^{\pm}$, $K^{\pm}$, p and $\bar{p}$ interactions on hydrogen: E. DeWolf et al., Nucl. Phys. B87 (1975) 325;

60 GeV/c pp: C. Bromberg, et al., Phys. Rev. D15 (1977) 64;

100 GeV/c pp: W. M. Morse et al., Phys. Rev. D15 (1977) 66;

100 GeV/c $\bar{p}p$: R. E. Ansorge et al., op. cit.; J. Whitmore, Phys. Reports 27C (1976);

12 GeV/c $\bar{p}p$: see Reference [10].

[13] P. Slattery, Phys. Rev. D7 (1973) 2073.

Table I

48.9 GeV/c $\bar{p}p$ elastic and topological cross sections, and inelastic charged multiplicity moments.

N_{charge}	Events found		Corrected Number[a]	Cross section (mb)
0	32		43	0.149 ± 0.039
2	2569	elastic	2255	7.81 ± 0.24
		inelastic	1643	5.69 ± 0.22
4	2556		2985	10.34 ± 0.20
6	2236		2675	9.27 ± 0.19
8	1564		1852	6.42 ± 0.16
10	693		821	2.85 ± 0.11
12	258		287	0.994 ± 0.067
14	62		83	0.288 ± 0.036
16	15		12	0.042 ± 0.017
18	2		2.5	0.009 ± 0.007
≥ 20	0		≤ 2.7[c]	≤ 0.009[c]
total	9987		12658	43.86 ± 0.25[b]

$$\langle n_c \rangle = 5.69 \pm 0.03$$

$$D \equiv (\langle n_c^2 \rangle - \langle n_c \rangle^2)^{\frac{1}{2}} = 2.71 \pm 0.02$$

$$\langle n_c \rangle / D = 2.10 \pm 0.02$$

$$\gamma \equiv \langle (n_c - \langle n_c \rangle)^3 \rangle / D^3 = 0.59 \pm 0.03$$

$$K \equiv \langle (n_c - \langle n_c \rangle)^4 \rangle / D^4 = 3.12 \pm 0.09$$

$$f_2^{cc} \equiv \langle n_c (n_c - 1) \rangle - \langle n_c \rangle^2 = 1.67 \pm 0.12$$

[a] Corrections are explained in the text.

[b] From Ref. [8].

[c] Upper limit at 90%. C.L.

Figure Captions

Fig. 1. Elastic differential cross sections, $d\sigma/dt$. The optical point is calculated from the total cross section of Ref. [8]. The fit, which is described in the text, does not include our two data points nearest to $t = 0$.

Fig. 2. $\bar{p}p$ total (σ_T), total inelastic (σ_{inel}), and topological cross sections (σ_n) as a function of laboratory beam momentum [10]. We show the upper limit at 90% confidence level for ≥ 20 prongs calculated from 0 events found in our experiment. The curves are to guide the eye.

Fig. 3. (a) Average charged multiplicity $\langle n_c \rangle$, (b) dispersion D, and (c) the ratio $\langle n_c \rangle / D$ as a function of laboratory beam momentum for $\bar{p}p$ and pp inelastic interactions [12]. The curves are to guide the eye.

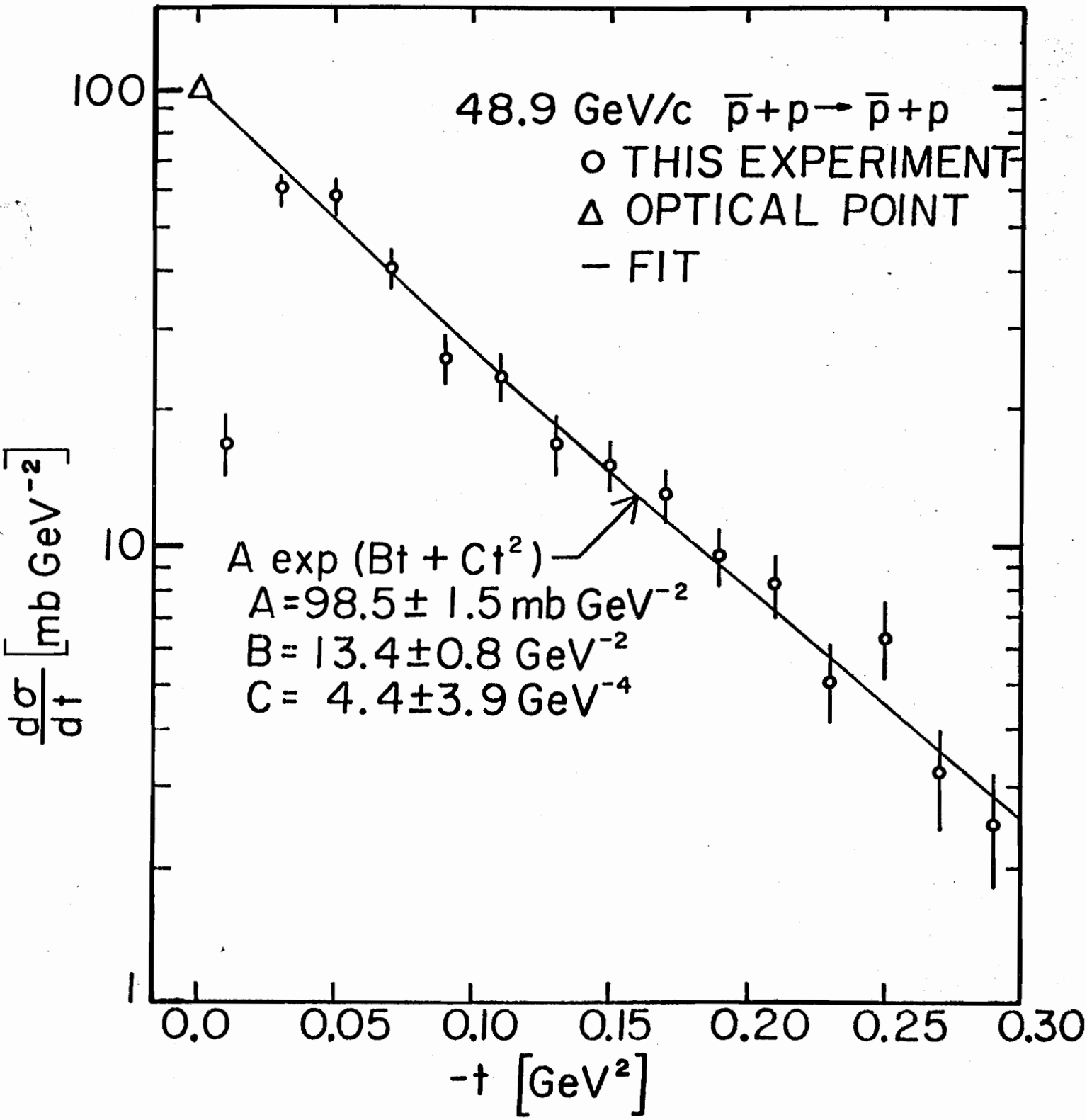
48.9 GeV/c $\bar{p}+p \rightarrow \bar{p}+p$
o THIS EXPERIMENT
Δ OPTICAL POINT
— FIT
A exp (Bt + Ct²)
A = 98.5 ± 1.5 mb GeV⁻²
B = 13.4 ± 0.8 GeV⁻²
C = 4.4 ± 3.9 GeV⁻⁴
100
10
1
0.0
0.05
0.10
0.15
0.20
0.25
0.30
$\frac{d\sigma}{dt}$ [mb GeV⁻²]
-t [GeV²]

Fig 1

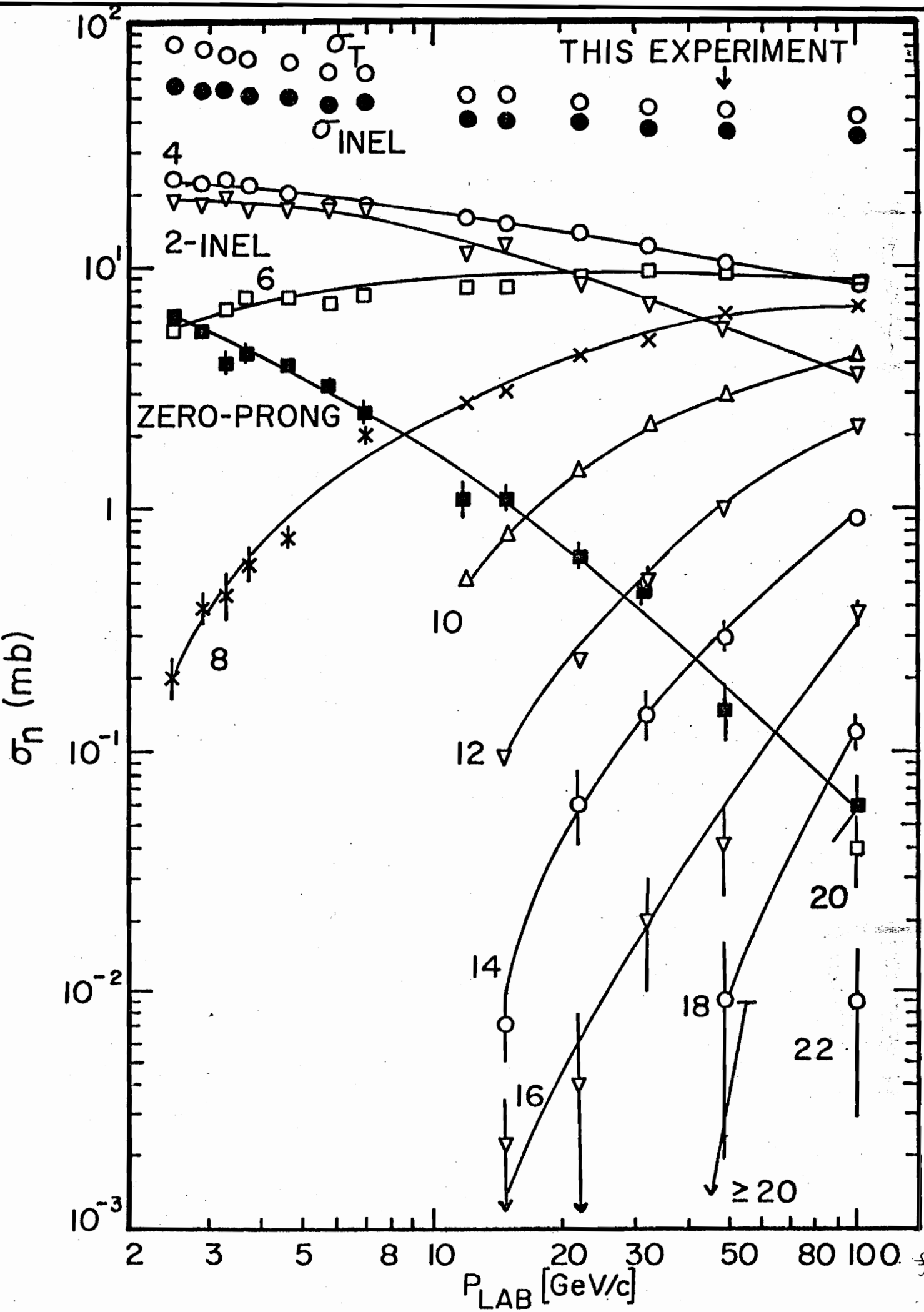
10^2
10^1
1
10^{-1}
10^{-2}
10^{-3}
σ_n (mb)
σ_T
σ_{INEL}
THIS EXPERIMENT
4
2-INEL
6
ZERO-PRONG
8
10
12
14
16
18
20
22
≥20
2
3
5
8
10
20
30
50
80
100
P_{LAB} [GeV/c]

Fig. 2

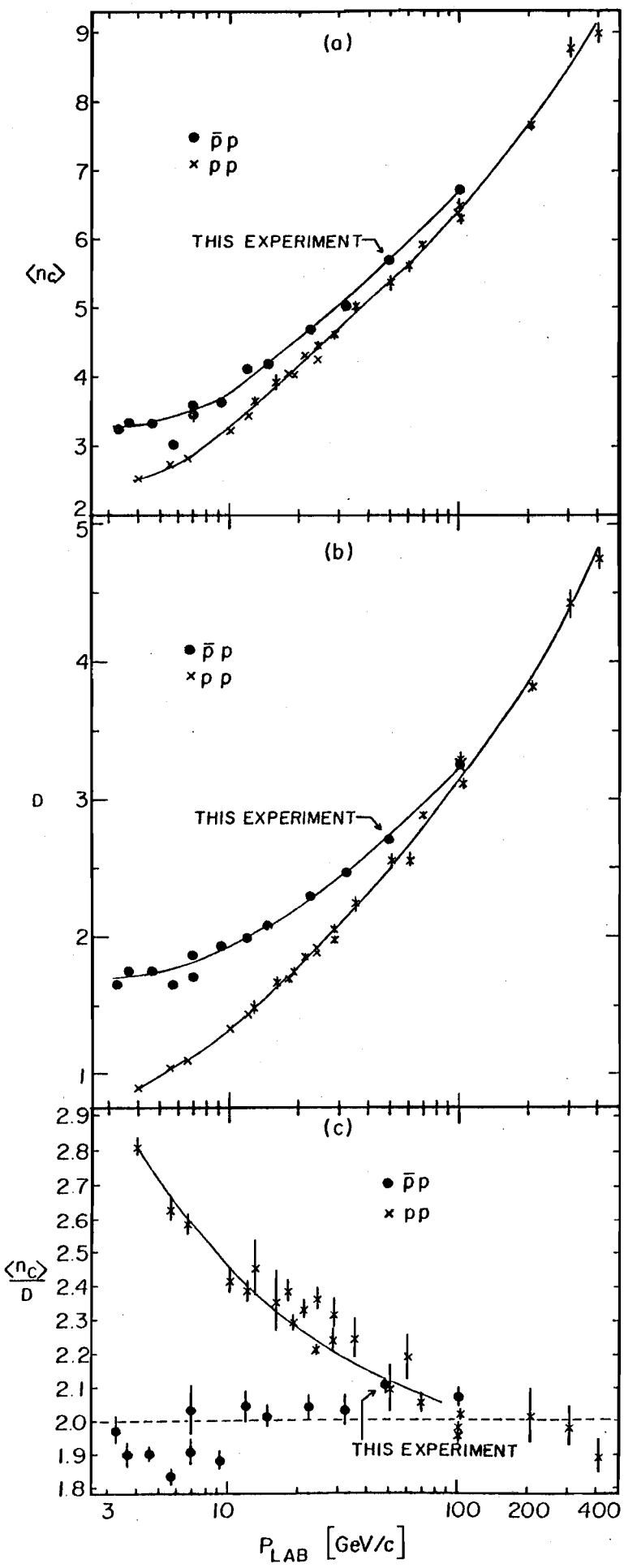
(a)
● p̄ p
× p p
THIS EXPERIMENT
⟨nc⟩
(b)
● p̄ p
× p p
THIS EXPERIMENT
D
(c)
● p̄ p
× p p
THIS EXPERIMENT
⟨nc⟩/D
PLAB [GeV/c]

Fig. 3